

Crystal Structure of the Human Myeloid Cell Activating Receptor TREM-1

Sergei Radaev,¹ Michael Kattah,¹ Bertha Rostro,¹ Marco Colonna,² and Peter D. Sun^{1,*}

¹Structural Immunology Section
Laboratory of Immunogenetics
National Institute of Allergy and
Infectious Diseases

National Institutes of Health
12441 Parklawn Drive
Rockville, Maryland 20852

²Department of Pathology and Immunology
Washington University School of Medicine
Box 8118
660 South Euclid Avenue
St. Louis, Missouri 63110

Summary

Triggering receptors expressed on myeloid cells (TREM) are a family of recently discovered receptors that play important roles in innate immune responses, such as to activate inflammatory responses and to contribute to septic shock in response to microbial-mediated infections. To date, two TREM receptors in human and several homologs in mice have been identified. We report the 2.6 Å resolution crystal structure of the extracellular domain of human TREM-1. The overall fold of the receptor resembles that of a V-type immunoglobulin domain with differences primarily located in the N-terminal strand. TREM-1 forms a “head-to-tail” dimer with 4100 Å² interface area that is partially mediated by a domain swapping between the first strands. This mode of dimer formation is different from the “head-to-head” dimerization that existed in V_HV_L domains of antibodies or V domains of T cell receptors. As a result, the dimeric TREM-1 most likely contains two distinct ligand binding sites.

Introduction

Triggering receptors expressed on myeloid cells (TREM) are a family of recently discovered activating receptors that may play important roles in myeloid cell-mediated inflammatory responses (Bouchon et al., 2000, 2001; Daws et al., 2001). The prototypic members of the family, TREM-1 and TREM-2, were identified in humans on chromosome 6 and are expressed on myeloid cells. More recently, three TREM-like transcripts, TLT-1, -2, and -3, were found in the TREM cluster on human chromosome 6 (Allcock et al., 2003). In mice, five activating forms, TREM-1 to TREM-5, and an inhibitory form, TLT-1, were found to reside on chromosome 17 (Chung et al., 2002; Washington et al., 2002). TREM-1 expression is found on monocytes and neutrophils and may contribute to the maturation of stem cells to monocytes (Gingras et al., 2002). Upon cross-linking, TREM-1 induces interleu-

kin-8 (IL-8) and myeloperoxidase secretion in neutrophils, and abundant release of IL-8, TNF- α , and other inflammatory mediators as well as chemotactic protein-1 (MCP-1) in monocytes. TREM-1 activation also induces Ca²⁺ influx and tyrosine phosphorylation of several proteins, particularly mitogen activated protein kinases ERK1 and ERK2. Expression of TREM-1 is upregulated in response to Toll-like receptor activation and is accompanied by an increased production of the proinflammatory cytokines TNF- α and GM-CSF, while production of the anti-inflammatory cytokine IL-10 is inhibited, suggesting a role for the receptor in acute inflammation (Bleharski et al., 2003). Excessive release of TNF- α , interleukin-1 β , and other proinflammatory cytokines and chemokines in response to infections is believed to cause sepsis syndrome-related multiple organ failure (Beutler et al., 1985; Glauser et al., 1991; Nathan and Ding, 2001). Interestingly, priming neutrophils and monocytes with lipopolysaccharide (LPS), lipoteichoic acid, heat-inactivated Gram-positive bacteria, Gram-negative bacteria, or fungi induces strong upregulation of TREM-1. In addition, TREM-1 was found on neutrophils isolated from the peritoneal cavity of patients or mice with bacterial septic shock. In contrast, little or no TREM-1 could be detected in nonmicrobial inflammatory lesions, such as psoriasis, ulcerative colitis, and vasculitis (Bouchon et al., 2001). Thus, TREM-1, with its synergistic activation during inflammation, may also contribute to the excessive inflammatory response during septic shock (Cohen, 2001; Nathan and Ding, 2001). Furthermore, mice treated with a murine TREM-1/IgG1-Fc fusion protein exhibited a partial protection against LPS-induced endotoxic shock, indicating the potential therapeutic significance of this type of treatment.

Like many other activating receptors that lack signaling components in their cytoplasmic tails, TREM-1 and -2 associate with the immunoreceptor tyrosine-based activation motif (ITAM)-containing molecule DAP12 through a charged residue in their transmembrane regions (Lanier et al., 1998). In contrast, TLT-1, -2, and -3 contain immunoreceptor tyrosine-based inhibitory motifs (ITIMs) in their cytoplasmic tails and thus may confer inhibitory functions (Allcock et al., 2003).

In general, TREMs show relatively low sequence identity (20%–30%) among them. The exceptions are human and mouse TREM-1 and mouse TREM-1 and TREM-3 which share 46% and 43% sequence identity, respectively. Structurally, the extracellular regions of all TREMs consist of a single V-type immunoglobulin (Ig)-like domain (Ig-V) of about 120 amino acids in length, followed by a neck region of about 70 amino acids. Despite intense efforts, the ligands of TREM receptors remain unknown. To better understand the function of this family of receptors, we have determined the crystal structure of the extracellular Ig-V domain of human TREM-1 at 2.6 Å resolution. Analysis of the TREM-1 structure and comparison to structures of other members of V-type Ig fold illustrate a unique “head-to-tail” receptor subunit association encompassing 4100 Å² interface area. This

*Correspondence: psun@nih.gov

Table 1. Data Collection, Phasing, and Refinement Statistics

Data Collection					
	Native	Se (Remote)	Se (Peak)	Se (Edge)	Au (Remote) ^a
Beamline	SBC-CAT	SER-CAT	SER-CAT	SER-CAT	SER-CAT
Wavelength (Å)	1.0376	0.9641	0.9790	0.9791	1.0246
Resolution limit (Å)	2.6	3.2	3.2	3.2	2.6
Unique reflections	23897(2369) ^b	11567(724)	12178(899)	13193(1319)	21585(1225)
Redundancy	4.2(4.2)	6.3(3.5)	6.8(4.0)	6.9(4.7)	3.4(1.9)
Completeness (%)	98.6(97.7)	90.3(56.1)	94.1(70.2)	99.8(99.2)	90.8(51.8)
R _{sym} (%) ^c	8.6(44.0)	16.3(48.7)	15.2(42.1)	15.8(44.2)	10.1(32.6)
<I/σ(I)>	23.5(4.2)	9.6(2.0)	12.2(2.7)	12.6(3.2)	14.1(1.9)
MAD Phasing SeMet (15.0–4.0 Å)					
Mean figure of merit	0.41				
MIR Phasing (15.0–3.0 Å)					
Mean figure of merit	0.25		Se (Peak)	Au (Remote)	
Phasing Power ^d			1.07	1.05	
R _{cutlis} (cen/acen) ^e			0.75/0.92	0.86/0.95	
Refinement					
Resolution (Å)	46–2.6				
No. reflections	22,801				
No. protein atoms	3928				
No. solvent atoms	229				
R _{cryst} (%)	20.1(32.3)				
R _{free} (%) ^f	25.1(37.6)				
Mean B factor (Å ²)	38				
Wilson B factor (Å ²)	47				
Rmsd bond lengths (Å)	0.007				
Rmsd bond angles (°)	1.67				

^a Data collected on KAu(CN)₂-soaked crystal.

^b Values in parentheses are for highest resolution shells: 2.6–2.7 Å (native), 3.1–3.2 Å (SeMet datasets), and 2.6–2.7 Å (KAu(CN)₂ remote).

^c R_{sym} = 100 × Σ|I_h - <I_h>|/ΣI_h, where <I_h> is the mean intensity of multiple measurements of symmetry equivalent reflections.

^d Phasing power = rms(F_h)/rms(E), where F_h is the calculated heavy-atom structure factor, and E is the phase-integrated lack of closure.

^e R_{cutlis} = Σ||F_{PH} ± F_P| - F_H|/Σ|F_{PH} ± F_P|, where F_P and F_{PH} are observed structure factors for the native and the derivative, and F_H is the calculated heavy-atom structure factor.

^f R_{free} was calculated using test set of 5%.

dimer formation is mediated, in part, by a domain swapping between the first strands of the monomers. The difference between the TREM-1 dimerization and the “head-to-head” dimerization mode observed for V domains of antibodies and T cell receptors may have implications to the function of TREM-1 receptor.

Results and Discussion

Structure Determination

The structure of the extracellular Ig-like domain of TREM-1, amino acids 17–133, was determined to 2.6 Å resolution by a combination of selenomethionone-based multiwavelength anomalous dispersion (MAD) and a gold-derivative-based single isomorphous replacement (SIR) methods to 2.6 Å resolution (Table 1). The crystals belong to a monoclinic space group P2₁ with cell dimensions a = 50.3, b = 128.6, c = 62.4 Å, and β = 101.7° and four molecules in each asymmetric unit. The refined crystallographic and free R factors are 20.1% and 25.1%, respectively. After refinement, the electron density map was contiguous in all four molecules from residue Glu 17 to Thr 133. The N-terminal Met 16 as well as Leu 134 and Glu 135, which are part of the C-terminal tag, were also visible in the electron density map.

Overall Structure

The overall structure of TREM-1 is similar to a typical Ig-V domain, which consists of nine strands forming two antiparallel β sheets locked together by a conserved disulfide bond between strands B and F (Figure 1). The first sheet is formed by the strands B-E-D-C’ and the second one by the strands A’-G’-F-C-C’. The four monomers in each asymmetric unit form two tightly associated dimers. Structural comparisons between TREM-1 and other members of Ig superfamily (IgSF) such as V_HV_L domains of IgG1, V_αV_β domains of T cell receptor (TCR) (Figure 1C), V_γV_δ TCR, CD8, and CTLA-4 result in 1.5–2.0 Å rms deviations for 76–83 superimposed C_α atoms. TREM-1, however, deviates from a classical Ig-V domain in the conformation of the first β strand. In a typical V-type Ig fold, the first strand breaks into two shorter strands, A and A’, where the strand A is hydrogen bonded to strand B of one β sheet and the A’, following a typical “strand switch,” pairs with strand G’ of the opposing β sheet. In the TREM-1 structure, strand A is distal to the core of the protein to form a parallel β sheet with strand B of the other monomer (Figure 2A). As a result, strand A’ pairs first with the G of the other monomer and then with G’ of itself. Recently, the structure of NK cell natural cytotoxicity receptor NKp44, from the

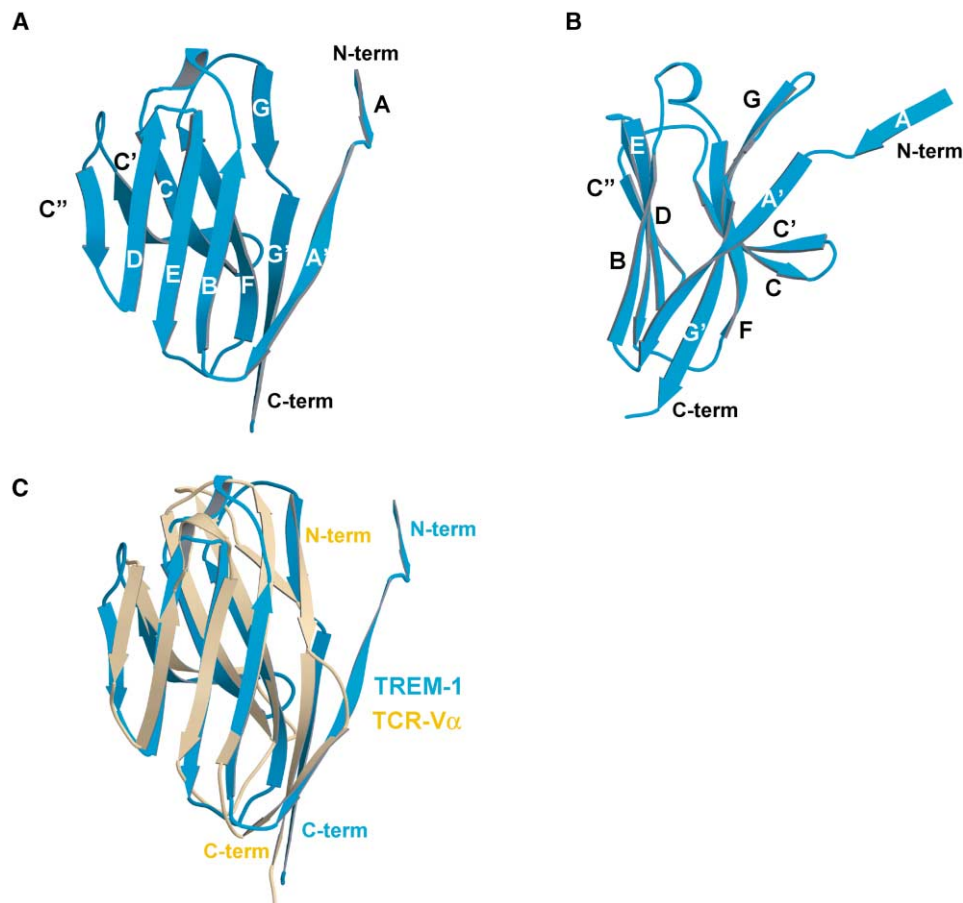


Figure 1. Ribbon Drawing of the TREM-1 Monomer

(A) Front view. All secondary structure elements on TREM-1 are marked in accordance with the sequence alignment in Figure 4.

(B) Side view of TREM-1. Molecule is rotated about 90° compare to the front view.

(C) Structural comparison between TREM-1 and V α domain of TCR. This figure and all subsequent ribbon drawings are prepared using the program MOLSCRIPT (Kraulis, 1991), and RASTER3D (Merritt and Bacon, 1997).

same gene cluster as TREMs (Allcock et al., 2003), was determined (Cantoni et al., 2003). NKp44 also displays a V-type Ig fold with an rms deviation of 1.3 Å to TREM-1 structure. However, unlike other members of the family, NKp44 contains a unique disulfide bond between C and C' strands. TREM-1 structure also has Cys 69 in its C' strand but lacks a complementary cysteine in C strand. Another feature of NKp44 that is different from other V-type Ig domains is the existence of a positively charged groove on its surface formed by C-C' and F-G strands. In addition, NKp44 does not form a dimer in solution and only a crystallographic dimer was observed in the NKp44 structure.

TREM-1 Dimer Formation

The extracellular Ig-V domain of TREM-1 exists as a dimer in solution as determined by size exclusion chromatography (data not shown). In the crystal, TREM-1 forms a noncrystallographic symmetry (NCS)-related dimer with the concave surfaces of the G-F-C-C' sheets of the two monomers facing each other (Figure 2A). An array of hydrogen bonds formed between the edge strands, A, A', and C' of one monomer and B, G, and

C' of the other extend the β sheet of each monomer into a contiguous barrel-like structure. The buried surface area between the two TREM-1 monomers is ~ 4100 Å², about twice the 1500–1600 Å² that is buried by V α V β antibody dimers or V α V β and V γ V δ of TCRs. The more than 2-fold increase in the buried surface with respect to antibody-like dimer is primarily due to the additional interactions between the swapped A and A' strands in TREM-1 (Bennett et al., 1995; Rousseau et al., 2003; Liu and Eisenberg, 2002). When the first 7 residues from strand A of TREM-1, which are involved in domain swapping, are removed, the buried surface area is reduced to about 2600 Å².

In addition to hydrogen bonds, the TREM-1 dimer is also stabilized by salt bridges and hydrophobic interactions. Specifically, there are two salt bridges between the opposing molecules at the dimer interface: Asp 60 to Arg 72, and Glu 62 to His 123 (Figure 2B). Prominent residues at the hydrophobic interface include Leu 18, Ala 20, Leu 24, Tyr 29, Val 39, Met 63, Pro 64, Tyr 116, Met 124, Leu 125, Phe 126, and Ile 129 of both monomers (Figure 2C). The two TREM-1 dimers in each asymmetric unit are related by a 2-fold noncrystallographic symme-

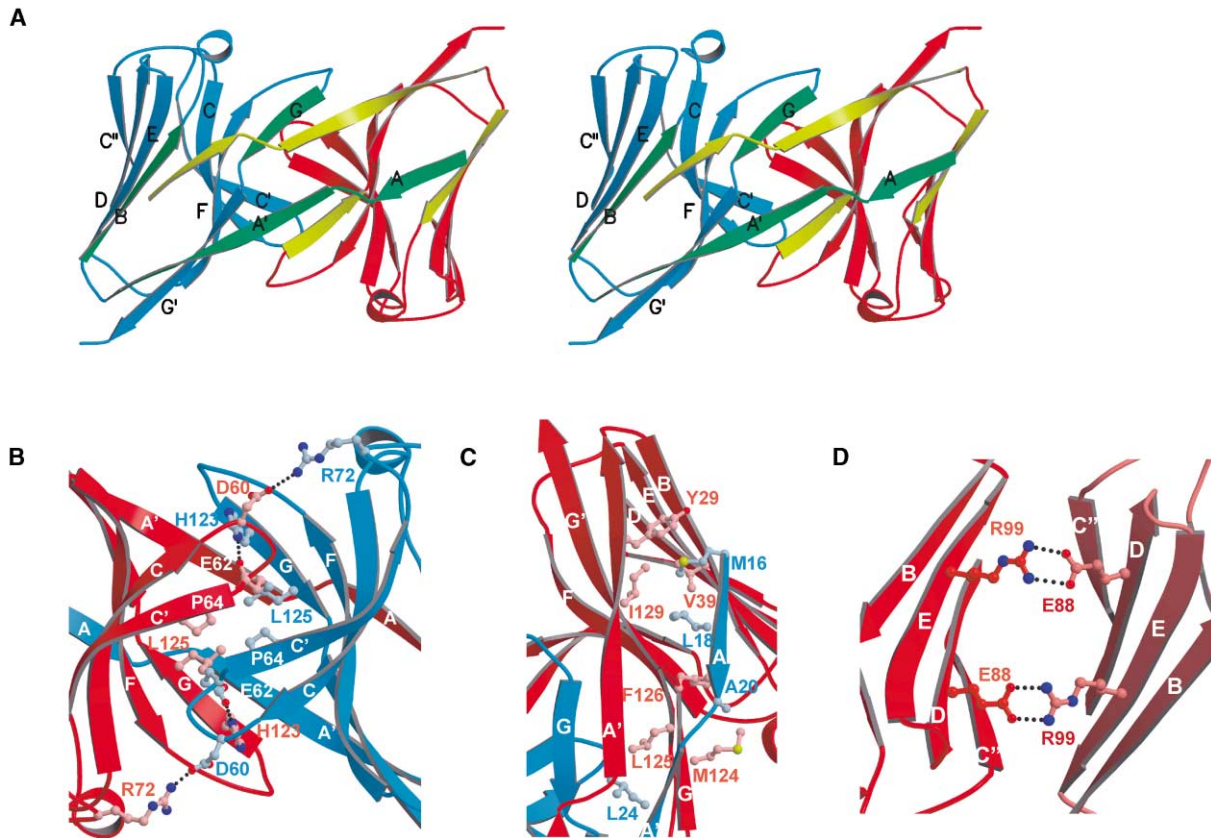


Figure 2. TREM-1 Dimer Interfaces

(A) Stereoview of TREM-1 dimer. Secondary structure elements involved in the interactions between N termini painted green in one monomer and yellow in another one.

(B) Detailed view of the hydrophobic core formed at the dimer interface by the N termini of TREM-1.

(C) Interactions between CC' regions of the monomers.

(D) Major interactions holding the two dimers. Residues participating in binding are shown as ball-and-sticks, color coded by strand color, except for oxygen (red), nitrogen (blue), and sulfur (yellow).

try (NCS) operator (Figure 2A). The surface area buried at this interface is about 1000 Å², which is significantly less than that buried between monomers. Two NCS-related salt bridges between Glu 88 of one dimer and Arg 99 of the other are found at this dimer-dimer interface (Figure 2D).

Comparison with Other Ig-V Dimers

It is worth noting that the physiological oligomerization state of TREM-1 is unknown. This is partly due to the low cell surface expression of the receptor in nonactivated myeloid cells and the lack of a stable transfected cell line. To address the dimerization of TREM-1, we compared the receptor structure with some of the known Ig-V dimers. The best-studied examples of the V-type Ig fold are structures of the variable domains of antibody Fab fragments and T cell antigen receptors (Harris et al., 1992; Cohen et al., 1996; Garboczi et al., 1996; Leahy et al., 1992; Ostrov et al., 2000). In both antibodies and TCRs, the Ig-V domains form a "head-to-head," parallel heterodimer with the "heads," CDR loops of each monomer, packing against each other opposite their C-terminal "tails" that do not pack closely together (Figure

3A). The largely hydrophobic dimer interface is formed by residues from the C, C', F, and G strands of each monomer (Figures 3 and 4). CD8 and CTLA-4 are two examples of homodimeric Ig-V dimers (Leahy et al., 1992; Ostrov et al., 2000). In the CD8 homodimer, dimer formation is nearly identical to that of antibody and TCR heterodimers with dimer interface residues conserved among them. CTLA-4, however, forms a disulfide-bonded dimer through a pair of membrane-proximal cysteines, and its structure displays a very different type of dimer formation as that of TCR (Figure 3B). The CTLA-4 dimer interface consists primarily of the A' and G strands near the C termini of the monomers. As a result, the CDR-like loops of the CTLA-4 dimer (BC, C'C'', and FG loops) are oriented in opposite directions, generating two separate ligand binding sites. The surface area buried in CTLA-4 homodimer interface is about 700 Å², significantly smaller than that in T cell receptors, antibodies, and CD8.

The most closely related example of a head-to-tail Ig-V dimer is the structure of a nonfunctional V δ homodimer (Li et al., 1998) (Figure 3C). However, there are significant structural differences observed between the V δ and TREM-1 dimers. In the V δ homodimer, major interac-

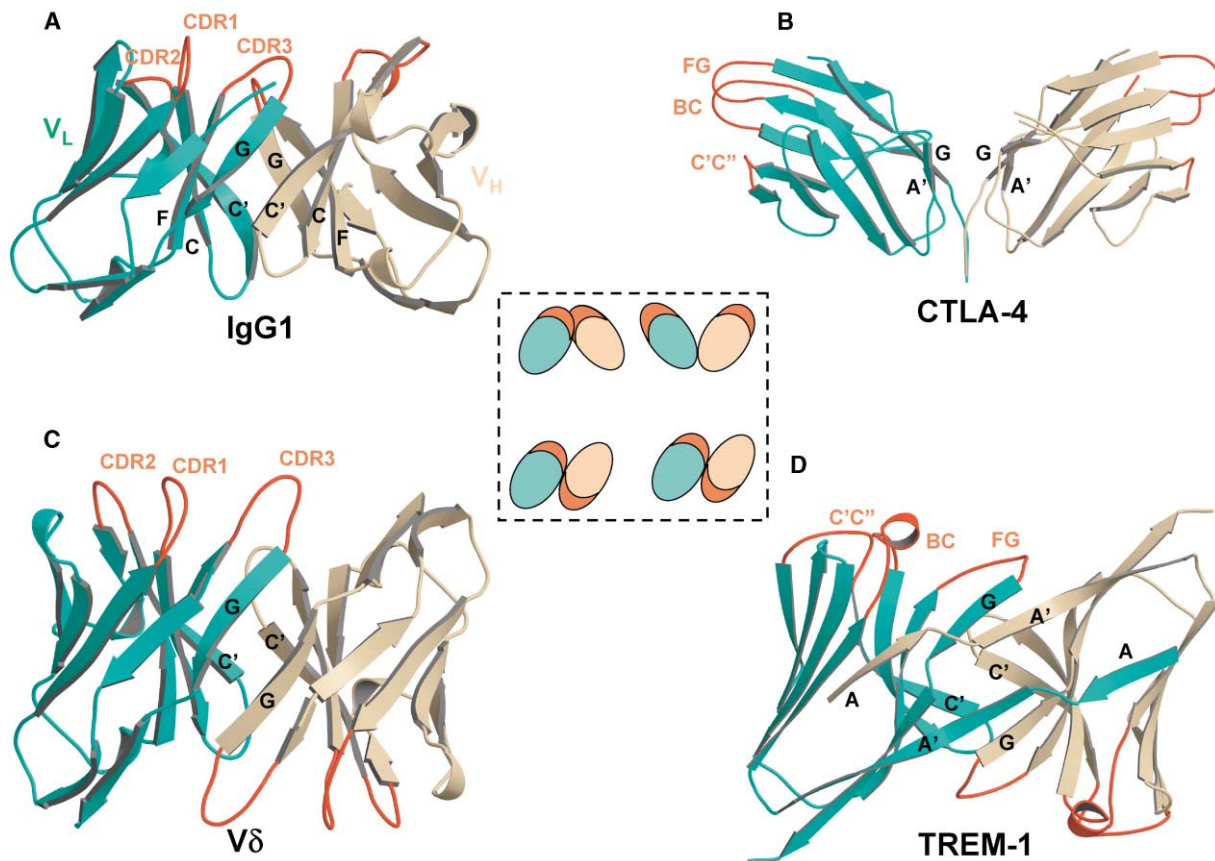


Figure 3. Several Examples of V-Type Domains Forming Homo- and Heterodimers
(A) $V_L V_H$ of mouse IgG1 (PDB accession code 3HFL). (B) CTLA-4 homodimer (PDB code 1I85). (C) V_δ homodimer (PDB accession code 1TVD). (D) TREM-1 homodimer. Complementarity determining regions (CDRs) are labeled; BC, C' C'' and FG loops correspond to CDR1, CDR2, and CDR3, respectively. Secondary structure elements involved in dimerization are labeled. Inset: cartoon representation of different dimer formation modes color coded to match ribbon models.

tions take place between G strands as well as between C' strands of the opposing monomers. The TREM-1 dimer, however, replaces the interface G strands of the V_δ with a swapped A and A' strands (Figure 3D). Since V_δ forms a nonfunctional dimer in the absence of V_γ , we investigated the possibility that the TREM-1 head-to-tail dimer may be artificial, due to the absence of the ~ 70 residue extracellular neck region that is C-terminal to the Ig-V domain. In the absence of structural information regarding the conformation of this neck region, we used several secondary structure prediction algorithms, including PSIPRED and SAM to assess the potential fold of this region (McGuffin et al., 2000; Karplus et al., 1998). All of them predict a lack of a defined fold in the neck region indicating a potential flexible domain. This suggests the neck domain is less likely to influence the V region dimer formation.

Next, we examined the interface residues of TREM-1 and other V-type IgSF dimers for their compatibility among different dimerization modes. When the structures of antibody-like dimers were compared with those of V_δ , CTLA-4, and TREM-1 homodimers, three interface residues appear to be particularly important in determining the mode of dimer formation. A Gln residue, conserved among antibodies and TCRs, at the end of the

C strand forms a hydrogen bond to the same Gln residue from the opposing monomer in most antibody-like V-type dimers (Figure 4). This Gln residue is changed to Lys in V_γ and Glu in V_δ that make a salt bridge in the structure of the $\gamma\delta$ TCR. In TREM-1 and V_δ homodimer isoleucine is found at the same position. The other two residues that appear to be important in mediating antibody-like dimerization are part of the interface hydrophobic core. One is located in the middle of the C' strand. In antibodies and TCRs, this residue is Leu, Phe, and Trp, whereas in CTLA-4 this residue is Glu, which makes formation of an antibody-like hydrophobic interface unfavorable. In TREM sequences, either Thr or Gln is found at this position. The other residue is located in the middle of F strand immediately preceding the conserved cysteine. It is either a leucine or tyrosine in antibody-like dimers. In TREM sequences, however, this residue becomes either Gln or Arg, which are less favorable for a hydrophobic interface. In addition, sequence comparison between human and mouse TREM-1 reveals that residues involved in TREM-1-like dimer formation are 60% conserved whereas those corresponding to $V_L V_H$ -type dimer formation are 40% conserved, suggesting that the antibody-like dimer is less favorable than TREM sequences.

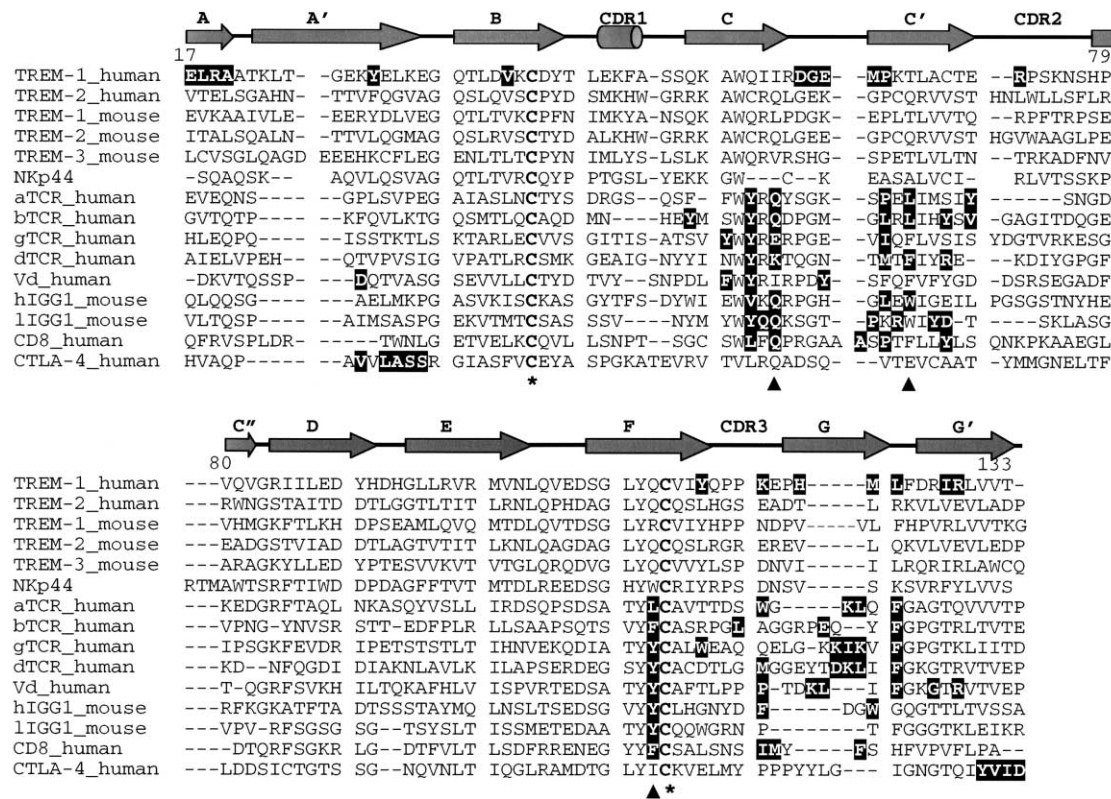


Figure 4. Structure-Based Sequence Alignment of Several TREMs and Other Members of the Ig-V Superfamily

The numbering is consistent with the mature sequence of human TREM-1. The secondary structure elements of TREM-1 are illustrated as arrows for β strands and cylinders for α helices. Residues involved in homo- and heterodimer formation are shown on black background. Cysteins making disulfide bonds conserved for V-type Ig fold are in bold and marked with asterisks. Gaps are indicated with (-). TREM-1 residues violating antibody-like dimer formation mode are marked with closed triangles.

To further evaluate the compatibility of TREM-1 with an antibody-like dimer, we superimposed TREM-1 monomer onto the structure of CD8 (Figure 5A). This anti-

body-like TREM-1 dimer buries $\sim 4000 \text{ \AA}^2$ interface area, which is only 100 \AA^2 smaller than the value observed for the TREM-1 dimer in the crystal structure. However,

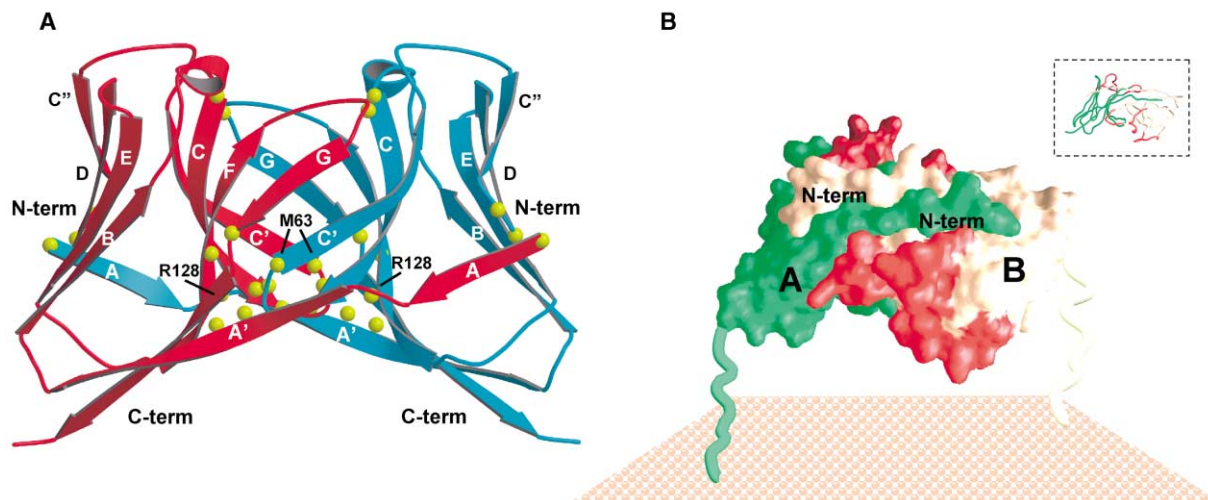


Figure 5. Hypothetical Structural Models of TREM-1

(A) TREM-1 structure modeled after CD8 homodimer. C_{α} atoms of residues making bad contacts ($<2.0 \text{ \AA}$) shown as yellow balls. (B) Cartoon representing TREM-1 dimer with the neck regions bound to the cell membrane. The molecular surface was created using GRASP (Nicholls et al., 1991). The potential ligand binding regions are shown in red. Worm drawing of TREM-1 dimer on the inset is given for orientation purposes.

there are numerous steric clashes between residues at the dimer interface of this model (Figure 5A). For example, both Met 63 and Arg 128 of TREM-1 are in close contact (<2.0 Å) to main chain atoms of the opposing monomer. In antibodies and TCRs, both residues are replaced by much smaller amino acids such as Ser, Gly, Pro, and Thr to avoid the steric hindrance at the dimer interface, suggesting that the sequence of TREM-1 is not compatible with an antibody-like dimer.

Finally, the TREM-1 dimerization mode was evaluated using the program SCORE, which calculates the compatibility of a given sequence to adopt a known protein-protein interaction mode based on the ability of its putative interface residues to form the salt bridges, hydrogen bonds, and hydrophobic interactions of a known template structure (Radaev et al., 2002). Using this algorithm, we first scored the propensity of V_{γ} and V_{δ} sequences of $\gamma\delta$ TCR to form the parallel antibody-like dimer versus the antiparallel V_{δ} homodimer. When the V_{γ} sequence is scored against either the $V_{\gamma}V_{\delta}$ heterodimer or V_{δ} homodimer crystal structures, the interface compatibility scores are 26 and 14, respectively. The higher score obtained for the antibody-like $V_{\gamma}V_{\delta}$ heterodimeric structure suggests that V_{γ} prefers parallel rather than the antiparallel dimeric structure. Conversely, if the V_{δ} sequence is scored against the same structural templates, the compatibility scores are 7 and 18 for the $V_{\gamma}V_{\delta}$ heterodimeric and V_{δ} homodimeric structure templates, respectively. This is consistent with the crystallographic result that V_{δ} alone prefers the homodimeric antiparallel structure (Li et al., 1998). When the TREM-1 sequence was evaluated using either the crystal structure or the CD8-like model of TREM-1 dimer as the template, the scores are 56 and 23 for the antiparallel and the parallel dimer, respectively, indicating a preference of TREM-1 sequence for the antiparallel dimer structure.

Potential Ligand Binding Site

Although the ligands of TREM-1 remain to be identified, we attempted to locate a putative ligand binding site on the receptor based on the known structures of Ig-V superfamily members and their modes of ligand binding. To date, the best-studied structures are those of antibodies and T cell antigen receptors (Harris et al., 1992; Gao et al., 1997; Stamper et al., 2001; Schwartz et al., 2001; Garboczi et al., 1996; Garcia et al., 1996). Other examples include the two T cell coreceptors CD8, which recognizes the nonpolymorphic $\alpha 3$ domain of MHC molecules, and CTLA-4, which binds B7-1 and B7-2 (Leahy et al., 1992; Ostrov et al., 2000). Despite their sequence and ligand diversity, antibodies TCRs, CD8, and CTLA-4 all recognize their cognate ligands using loops that are topologically identical to antibody CDRs. The use of a set of common ligand binding regions among otherwise diverse Ig-V domains suggests that these loops are crucial for ligand recognition by members of this superfamily. Thus, it is conceivable that TREM-1 also captures its ligand with its CDR-equivalent loop regions. The unique dimer structure of TREM-1, however, predicts two separate ligand binding sites as compared to antibodies TCR and CD8 which contain only one binding site (Figure

3D). This is reminiscent of the structure of CTLA-4/B7-1 (B7-2) complexes in which each CTLA-4 monomer binds one B7 molecule and the two ligand binding sites point away from each other in the CTLA-4 dimer (Figure 3B). The TREM-1 head-to-tail dimer would also require the receptor to adopt a different orientation with respect to the membrane compared to head-to-head dimers (Figure 5B).

In summary, the structure of TREM-1 reveals a unique head-to-tail mode of dimerization different from other known Ig-V domain structures. The dimer interface is approximately twice the size of antibody-like Ig-V dimers and involves strand swapping between the first strands of the monomers. This unique dimer formation likely creates two separate ligand binding sites for each TREM-1 receptor dimer. However, further investigations, including the identification of TREM-1 ligands and the solution of the TREM-1/ligand complex structure, are needed to gain a better understanding of the function of TREM-1 and its role in innate immune response.

Experimental Procedures

Protein Expression, Purification, and Crystallization

The extracellular part of human TREM-1 receptor (residues 17–133 of mature sequence) was subcloned into a pET-22b vector using NdeI and XhoI restriction sites. The recombinant protein was expressed in *Escherichia coli* BL21 (DE3) cells as inclusion bodies and then reconstituted in vitro. Cells were grown at 37°C in 10 liters of Luria-Bertani broth using a New Brunswick Bioflo 3000 Bioreactor (New Brunswick Scientific Co., Inc., Edison, NJ) vessel and induced with 0.5 mM IPTG at an approximate OD_{596} of 1.7 for 4 hr. The inclusion bodies were isolated by repeated washing with buffer containing 2 M urea. Prior to refolding, the inclusion bodies were redissolved in 6 N guanidine hydrochloride, 2 mM DTT, and 50 mM sodium phosphate at pH 6. The refolding was initiated by a quick dilution of dissolved inclusion bodies into a refolding buffer consisting of 0.5 M L-arginine, 2.5 mM oxidized glutathione, 5 mM reduced glutathione, 10 μ g/ml AEBF (4-[2-(aminoethyl)]-benzenesulfonyl fluoride hydrochloride), and 100 mM Tris at pH 8.0 and then dialyzed thoroughly against water. The renatured TREM-1 was concentrated on a Ni-NTA affinity column (Qiagen, Inc., Valencia, California) and was further purified on a Superdex 200 size-exclusion column (Amersham Biosciences, Piscataway, New Jersey). Refolded TREM-1 eluted as a dimer on the size-exclusion column with an approximate molecular weight of 30 kDa. The identity of the refolded protein was confirmed by N-terminal amino acid sequencing and electrospray ionization mass spectrometry (ESI-MS). The selenomethionine (SeMet) derivative of TREM-1 was prepared under altered bacterial growth conditions (Van Duyne et al., 1993). In brief, bacteria inoculum (40 ml) containing the TREM-1 expression plasmid was grown at 37°C in LB broth overnight. The LB broth in the overnight inoculum was replaced with M9 medium supplemented with 0.4% glucose, 0.1 mM $CaCl_2$, and 3 mM $MgSO_4$ and distributed into four 1 liter shaker flasks at 37°C. The bacteria cell culture was induced at an approximate OD_{596} of 0.6 with 0.5 mM IPTG for 12 hr together with added 50 mg per liter each of the amino acids Leu, Ile, and Val, and 100 mg per liter each of Thr, Lys, Phe, and SeMet. Refolding of the SeMet-modified TREM-1 was the same as for the native protein. The presence of four SeMet residues was confirmed by ESI-MS.

Single crystals were obtained by vapor diffusion in hanging drops at room temperature using reservoir solutions containing 2.1–2.4 M ammonium sulfate and 100 mM MES or sodium citrate at pH 5.4–5.7. Crystals appeared after 1–3 days and grew to an average size of $0.1 \times 0.04 \times 0.02$ mm in approximately 2 weeks. Crystals grown using sodium citrate buffer were typically larger and had the same morphology as those grown using MES, but displayed nonisotropic and streaking diffraction only to 3.5 Å upon freezing. As a result, only those crystals obtained in MES buffer were used for structure

solution. Following brief soaking in a solution containing 1.8 M ammonium sulfate, 100 mM Li_2SO_4 , 100 mM MES, pH 5.7, and 20% glycerol, crystals were flash frozen in a liquid nitrogen stream. ESI-MS was utilized to facilitate the search for possible heavy-metal derivatives (Sun and Hammer, 2000). Heavy-metal solutions were mixed with the protein in crystallization buffer, incubated for 30 min to several hours, and analyzed by mass spectrometry.

Structure Determination

Multiwavelength anomalous diffraction (MAD) data sets from SeMet TREM-1 crystal and from native TREM-1 crystal quick soaked for 10 min in saturated solution of $\text{KAu}(\text{CN})_2$ (Sun et al., 2002; Sun and Radaev, 2002) were collected at Southeast Regional Collaborative Access Team (SER-CAT) 22-ID beamline at the Advanced Photon Source, Argonne National Laboratory. The native data set was collected at SBC-CAT beamline. Supporting institutions are listed at www.ser.anl.gov/new/members.html. The data were processed and scaled with HKL2000 (Otwinowski and Minor, 1997). The crystals belong to the monoclinic space group $P2_1$, with cell dimensions $a = 50.3$, $b = 128.6$, $c = 62.4$ Å, and $\beta = 101.7^\circ$ and contain four molecules per asymmetric unit. Ten out of sixteen Se sites were located by the program SOLVE (Terwilliger and Berendzen, 1999) using diffraction data from 15–4 Å. Consecutive density modification with 2-fold NCS averaging and phase extension to 2.8 Å with the program DM (Cowtan and Main, 1996) followed by solvent flipping by SOLOMON (Abrahams and Leslie, 1996) from CCP4 program suite (CCP4, 1994) resulted in an electron density map that showed recognizable secondary structure elements but remained difficult to trace. Phases calculated from this electron density map were used to locate a single heavy-metal site in a difference Fourier map calculated between the $\text{KAu}(\text{CN})_2$ derivative (remote wavelength) and the native dataset. MIR phases were then calculated using the remote wavelength of $\text{KAu}(\text{CN})_2$ and the peak wavelength of the SeMet derivatives with MLPHARE (CCP4, 1994), and subsequently combined with the MAD phases of the SeMet derivative from SOLVE. Density modification including NCS averaging, solvent flipping, and incremental phase extension to 2.8 Å resulted in an improved and interpretable electron density map. The program "O" was used for model building and adjustment (Kleywegt and Jones, 1997). Positional and individual B factor refinement of the native dataset was carried out using the maximum likelihood target function of CNS v1.0 (Brunger et al., 1998). Due to the high ammonium sulfate content (2.1–2.4 M) in the crystallization buffer, ten sulfate ions were built into densities near positively charged arginine and lysine residues. In addition, a well-defined glutathione molecule was built into one of the four TREM monomers in the asymmetric unit, forming a disulfide bond to Cys 69. Surface areas were calculated with the program SURFACE as part of the CCP4 program suite using a probe radius of 1.4 Å (Chothia, 1975).

Acknowledgments

We thank C. Hammer and M. Garfield for mass spectroscopy measurements and N-terminal amino acid sequencing; J. Johnson, Z. Dauter, and J. Chrzas for their help with X-ray synchrotron data collection; and J. Boyington and C. Foster for their valuable comments on the manuscript. The use of the Advanced Photon Source was supported by the US Department of Energy, Basic Energy Sciences, Office of Science, under Contract No. W-31-109-Eng-38. This work is supported by the intramural research funding from the National Institute of Allergy and Infectious Diseases.

Received: July 16, 2003

Revised: August 27, 2003

Accepted: September 3, 2003

Published: December 2, 2003

References

Abrahams, J.P., and Leslie, A.G.W. (1996). Methods used in the structure determination of bovine mitochondrial F1 ATPase. *Acta Crystallogr. D* 52, 30–42.

Allcock, R.J., Barrow, A.D., Forbes, S., Beck, S., and Trowsdale,

J. (2003). The human TREM gene cluster at 6p21.1 encodes both activating and inhibitory single IgV domain receptors and includes NKp44. *Eur. J. Immunol.* 33, 567–577.

Bennett, M.J., Schlunegger, M.P., and Eisenberg, D. (1995). 3D domain swapping: a mechanism for oligomer assembly. *Protein Sci.* 4, 2455–2468.

Beutler, B., Milsark, I.W., and Cerami, A.C. (1985). Passive immunization against cachectin/tumor necrosis factor protects mice from lethal effect of endotoxin. *Science* 229, 869–871.

Bleharski, J.R., Kiessler, V., Buonsanti, C., Sieling, P.A., Stenger, S., Colonna, M., and Modlin, R.L. (2003). A role for triggering receptor expressed on myeloid cells-1 in host defense during the early-induced and adaptive phases of the immune response. *J. Immunol.* 170, 3812–3818.

Bouchon, A., Dietrich, J., and Colonna, M. (2000). Cutting edge: inflammatory responses can be triggered by TREM-1, a novel receptor expressed on neutrophils and monocytes. *J. Immunol.* 164, 4991–4995.

Bouchon, A., Facchetti, F., Weigand, M.A., and Colonna, M. (2001). TREM-1 amplifies inflammation and is a crucial mediator of septic shock. *Nature* 410, 1103–1107.

Brunger, A.T., Adams, P.D., Clore, G.M., DeLano, W.L., Gros, P., Grosse-Kunstleve, R.W., Jiang, J.-S., Kuszewski, J., Nilges, N., Pannu, N.S., et al. (1998). Crystallography & NMR system (CNS): a new software system for macromolecular structure determination. *Acta Crystallogr. D* 54, 905–921.

Cantoni, C., Ponassi, M., Biassoni, R., Conte, R., Spallarossa, A., Moretta, A., Moretta, L., Bolognesi, M., and Bordo, D. (2003). The three-dimensional structure of the human NK cell receptor NKp44, a triggering partner in natural cytotoxicity. *Structure* 11, 725–734.

CCP4 (Collaborative Computational Project) (1994). The CCP4 suite: programs for protein crystallography. *Acta Crystallogr. D* 50, 760–763.

Chothia, C. (1975). Structural invariants in protein folding. *Nature* 254, 304–308.

Chung, D.H., Seaman, W.E., and Daws, M.R. (2002). Characterization of TREM-3, an activating receptor on mouse macrophages: definition of a family of single Ig domain receptors on mouse chromosome 17. *Eur. J. Immunol.* 32, 59–66.

Cohen, J. (2001). TREM-1 in sepsis. *Lancet* 358, 776–778.

Cohen, G.H., Sheriff, S., and Davies, D. (1996). Refined structure of the monoclonal antibody HyHEL-5 with its antigen hen egg-white lysozyme. *Acta Crystallogr. D* 52, 315–326.

Cowtan, K., and Main, P. (1996). Phase combination and cross validation in iterated density-modification calculations. *Acta Crystallogr. D* 52, 43–48.

Daws, M.R., Lanier, L.L., Seaman, W.E., and Ryan, J.C. (2001). Cloning and characterization of a novel mouse myeloid DAP12-associated receptor family. *Eur. J. Immunol.* 31, 783–791.

Gao, G.F., Tormo, J., Gerth, U.C., Wyer, J.R., McMichael, A.J., Stuart, D.I., Bell, J.I., Jones, E.Y., and Jakobsen, B.K. (1997). Crystal structure of the complex between human CD8alpha(alpha) and HLA-A2. *Nature* 387, 630–634.

Garboczi, D.N., Ghosh, P., Utz, U., Fan, Q.R., Biddison, W.E., and Wiley, D.C. (1996). Structure of the complex between human T-cell receptor, viral peptide and HLA-A2. *Nature* 384, 134–141.

Garcia, K.C., Degano, M., Stanfield, R.L., Brunmark, A., Jackson, M.R., Peterson, P.A., Teyton, L., and Wilson, I.A. (1996). An alpha beta T cell receptor structure at 2.5 Å and its orientation in the TCR-MHC complex. *Science* 274, 209–219.

Gingras, M.C., Lapillonne, H., and Margolin, J.F. (2002). TREM-1, MDL-1, and DAP12 expression is associated with a mature stage of myeloid development. *Mol. Immunol.* 38, 817–824.

Glauser, M.P., Zanetti, G., Baumgartner, J.D., and Cohen, J. (1991). Septic shock: pathogenesis. *Lancet* 338, 732–736.

Harris, L.J., Larson, S.B., Hasel, K.W., Day, J., Greenwood, A., and McPherson, A. (1992). The three-dimensional structure of an intact monoclonal antibody for canine lymphoma. *Nature* 360, 369–372.

- Karplus, K., Barrett, C., and Hughey, R. (1998). Hidden Markov models for detecting remote protein homologies. *Bioinformatics* *14*, 846–856.
- Kleywegt, G.J., and Jones, T.A. (1997). Model-building and refinement practice. *Methods. Enzymol.* *277*, 208–230.
- Kraulis, P. (1991). MOLSCRIPT: a program to produce both detailed and schematic plots of protein structures. *J. Appl. Crystallogr.* *24*, 946–950.
- Lanier, L.L., Corliss, B.C., Wu, J., Leong, C., and Phillips, J.H. (1998). Immunoreceptor DAP12 bearing a tyrosine-based activation motif is involved in activating NK cells. *Nature* *391*, 703–707.
- Leahy, D.J., Axel, R., and Hendrickson, W.A. (1992). Crystal structure of a soluble form of the human T cell coreceptor CD8 at 2.6 Å resolution. *Cell* *68*, 1145–1162.
- Li, H., Lebedeva, M.I., Llera, A.S., Fields, B.A., Brenner, M.B., and Mariuzza, R.A. (1998). Structure of the Vdelta domain of a human gammadelta T-cell antigen receptor. *Nature* *391*, 502–506.
- Liu, Y., and Eisenberg, D. (2002). 3D domain swapping: as domains continue to swap. *Protein Sci.* *11*, 1285–1299.
- McGuffin, L.J., Bryson, K., and Jones, D.T. (2000). The PSIPRED protein structure prediction server. *Bioinformatics* *16*, 404–405.
- Merritt, E.A., and Bacon, D.J. (1997). Raster3D: photorealistic molecular graphics. *Methods Enzymol.* *277*, 505–524.
- Nathan, C., and Ding, A. (2001). TREM-1: a new regulator of innate immunity in sepsis syndrome. *Nat. Med.* *7*, 530–532.
- Nicholls, A., Sharp, K.A., and Honig, B. (1991). Protein folding and association: insights from the interfacial and thermodynamic properties of hydrocarbons. *Proteins* *11*, 281–296.
- Ostrov, D.A., Shi, W., Schwartz, J.C., Almo, S.C., and Nathenson, S.G. (2000). Structure of murine CTLA-4 and its role in modulating T cell responsiveness. *Science* *290*, 816–819.
- Otwinowski, Z., and Minor, W. (1997). Processing of X-ray diffraction data collected in oscillation mode. *Methods Enzymol.* *276*, 307–326.
- Radaev, S., Kattah, M., Zou, Z., Colonna, M., and Sun, P.D. (2002). Making sense of the diverse ligand recognition by NKG2D. *J. Immunol.* *169*, 6279–6285.
- Rousseau, F., Schymkowitz, J.W.H., and Itzhaki, L.S. (2003). The unfolding story of three-dimensional domain swapping. *Structure* *11*, 243–251.
- Schwartz, J.C., Zhang, X., Fedorov, A.A., Nathenson, S.G., and Almo, S.C. (2001). Structural basis for co-stimulation by the human CTLA-4/B7-2 complex. *Nature* *410*, 604–608.
- Stamper, C.C., Zhang, Y., Tobin, J.F., Erbe, D.V., Ikemizu, S., Davis, S.J., Stahl, M.L., Seehra, J., Somers, W.S., and Mosyak, L. (2001). Crystal structure of the B7-1/CTLA-4 complex that inhibits human immune responses. *Nature* *410*, 608–611.
- Sun, P.D., and Hammer, C.H. (2000). Mass-spectrometry assisted heavy-atom derivative screening of human FcgRIII crystals. *Acta Crystallogr. D* *56*, 161–168.
- Sun, P.D., and Radaev, S. (2002). Generating isomorphous heavy-atom derivatives by a quick-soak method. Part II: phasing of new structures. *Acta Crystallogr. D* *58*, 1099–1103.
- Sun, P.D., Radaev, S., and Kattah, M. (2002). Generating isomorphous heavy-atom derivatives by a quick-soak method. Part I: test cases. *Acta Crystallogr. D* *58*, 1092–1098.
- Terwilliger, T.C., and Berendzen, J. (1999). Automated structure solution for MIR and MAD. *Acta Crystallogr. D* *55*, 849–861.
- Van Duyn, G.D., Standaert, R.F., Karplus, P.A., Schreiber, S.L., and Clardy, J. (1993). Atomic structures of the human immunophilin FKBP-12 complexes with FK506 and rapamycin. *J. Mol. Biol.* *229*, 105–124.
- Washington, A.V., Quigley, L., and McVicar, D.W. (2002). Initial characterization of TREM-like transcript (TLT)-1: a putative inhibitory receptor within the TREM cluster. *Blood* *100*, 3822–3824.